# PHOTOELASTIC STRESS INTENSITY FACTOR DETERMINATION FOR CIRCULAR-SECTOR CRACKS

C.L. Chow and C.W. Woo
Department of Mechanical Engineering,
University of Hong Kong

## ABSTRACT

The mixed-mode stress intensity factors for different circular-sector cracks in a rectangular plate under uniform loading are photoelastically determined. The angle enclosed within the circular-sector crack extends from 120 to 180 degrees.

The mixed-mode singular stress equations at the crack tip for a circular-sector crack and an inclined straight crack are the same. The far-field maximum shear stresses based on the exact solution for the crack configurations are however different. This paper presents two methods of analysis for the determination of the stress intensity factors for the circular-sector cracks.

## INTRODUCTION

The concept of linear elastic fracture mechanics has been widely accepted as an important engineering tool for characterizing material behaviour in the presence of a crack or flaw. The application of fracture mechanics technology in engineering design is furthered by the availability of increasing number of experimental methods to determine the stress intensity factor [1, 2] for which analytical solution may be difficult, if not impossible to achieve.

Of the experimental methods, photoelasticity has gained increasing popularity in recent years for the stress intensity factor characterization under pure mode I and mixed-mode loadings[3-8]. Because of the mathematical complexities, the crack configurations considered in the past are often idealized to straight cracks. The straight cracks are however rarely found in engineering structures. The curved cracks have received little attention by the fracture mechanics researchers and these cracks have so



far been confined to infinite medium (1). This paper describes two methods of analysis which extend the application of the photoelastic stress intensity factor determination to circular-sector cracks in a finite width and length plates as shown in Fig. 1. The angle enclosed by the circular-sector crack extends from 120 to 180 degrees. Examples of the cracks observed in the practical engineering structures include weld-joints, in the tyre-testing road wheels, turbine bore-holes, etc.

## THEORY

Consider an infinite plate with a circular-sector crack of unit radius (R = 1) subjected to uniaxial tension $\sigma_o$ at infinity (Fig. 1). The stress

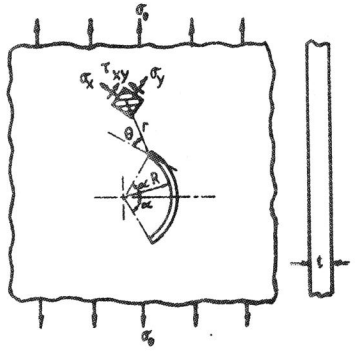


Figure 1 An Infinite Plate With Circular-Sector Crack Under Uniaxial Tension

components for the crack due to Muskhelishvili (9) are given by:

$$\sigma_x + \sigma_y = 2[\phi(z) + \overline{\phi(z)}]$$

$$(\sigma_y - \sigma_x) + 2i\,\tau_{xy} = 2[\bar{z}\,\phi'(z) + \psi(z)] \qquad (1)$$

where $\phi(z)$ and $\psi(z)$ are Muskhelishvili's potential functions, $\sigma_x$, $\sigma_y$ and $\tau_{xy}$ are respectively x-direction stress, y-direction stress and shear stress. Hence the stresses computed from the analytical solution of Equation (1) are exact, representing the stress state both in the "singular" and "far-field" regions of the crack tip.

With the transformation of $z = e^{i\alpha} + re^{i(\alpha-\theta)}$, Equation (1) may be expressed in the form of singular term equations as:

$$\sigma_x = \frac{K_1}{\sqrt{2\pi r}} \cos\frac{\theta}{2}\left(1 - \sin\frac{\theta}{2}\sin\frac{3\theta}{2}\right) - \frac{K_2}{\sqrt{2\pi r}} \sin\frac{\theta}{2}\left(2 + \cos\frac{\theta}{2}\cos\frac{3\theta}{2}\right)$$

$$\sigma_y = \frac{K_1}{\sqrt{2\pi r}} \cos\frac{\theta}{2}\left(1 + \sin\frac{\theta}{2}\sin\frac{3\theta}{2}\right) + \frac{K_2}{\sqrt{2\pi r}} \sin\frac{\theta}{2}\cos\frac{\theta}{2}\cos\frac{3\theta}{2} \qquad (2)$$

$$\tau_{xy} = \frac{K_1}{\sqrt{2\pi r}} \sin\frac{\theta}{2}\cos\frac{\theta}{2}\cos\frac{3\theta}{2} + \frac{K_2}{\sqrt{2\pi r}} \cos\frac{\theta}{2}\left(1 - \sin\frac{\theta}{2}\sin\frac{3\theta}{2}\right)$$

where the stress intensity factors are

$$K_1 = \frac{\sigma_o\sqrt{\pi\sin\alpha}}{2}\left\{\left[1 + \frac{\sin^2\frac{\alpha}{2}\cos^2\frac{\alpha}{2}}{1 + \sin^2\frac{\alpha}{2}}\right]\cos\frac{\alpha}{2} - \cos\frac{3\alpha}{2}\right\}$$

$$K_2 = \frac{\sigma_o\sqrt{\pi\sin\alpha}}{2}\left\{\sin\frac{3}{2}\alpha - \frac{\sin\frac{\alpha}{2}\left(1 + \sin^2\frac{\alpha}{2}\cos^2\frac{\alpha}{2}\right)}{1 + \sin^2\frac{\alpha}{2}}\right\} \qquad (3)$$

where $K_1$ and $K_2$ are mode I and II stress intensity factors respectively, r is radial distance to the crack tip, $\theta$ is angle of rotation at the crack tip as shown in Fig. 1, and $\alpha$ is half-angle of a circular arc.

As the isochromatic fringe order generated photoelastically are proportional to the maximum shear stress, it is therefore desirable to express various stress components shown in Equation (1) in the form of the maximum shear stress $\tau_{max}$ as

$$\tau_{max} = \frac{1}{2}\left[(\sigma_x - \sigma_y)^2 + 4\tau_{xy}^2\right]^{\frac{1}{2}} \qquad (4)$$

The maximum shear stress can be obtained from the measured photoelastic fringe order N by the stress-optic law as

$$\tau_{max} = \frac{Nf}{2t} \qquad (5)$$

where f is the material fringe value and t is the plate thickness.

Substituting Equation (2) into Equation (4), we obtain

$$\tau_{max} = \frac{1}{2(2\pi r)^{\frac{1}{2}}}\left[(K_1\sin\theta + 2K_2\cos\theta)^2 + (K_2\sin\theta)^2\right]^{\frac{1}{2}} \qquad (6)$$

The above equation may be represented graphically as shown in Fig. 2



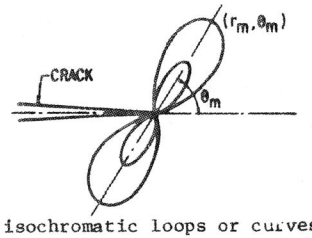


Figure 2
Isochromatic Loop
Close To the Crack
Tip

in terms of the isochromatic loops or curves of constant $\tau_{max}$. For each isochromatic loop there is an angle $\theta_m$ for which the isochromatic loop reaches the largest radius $r_m$. By differentiating the maximum shear stress of Equation (6) with respect to the angle , the resulting singular-term equation becomes

$$\left(\frac{K_2}{K_1}\right)^2 - \frac{4}{3}\left(\frac{K_2}{K_1}\right)\cos 2\theta_m - \frac{1}{3} = 0 \qquad (7)$$

As Equations (6) and (7) describe the stress state at close vicinity of the crack tip, they are applicable to the stresses measured away from the crack tip or for large value of r.

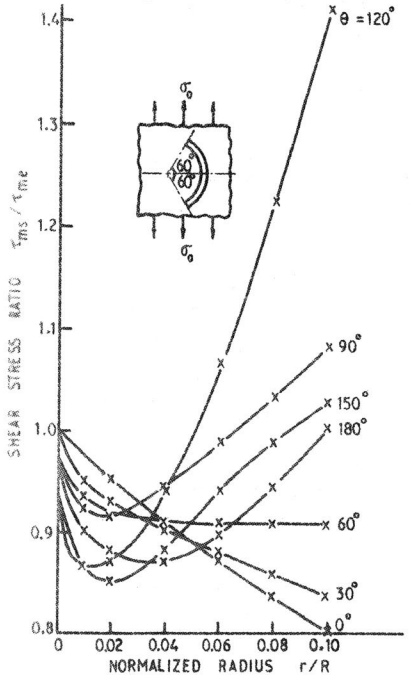


Figure 3 Variation of Shear Stress Ratio Versus Normalized Radius for $\alpha$ = 60 Deg.

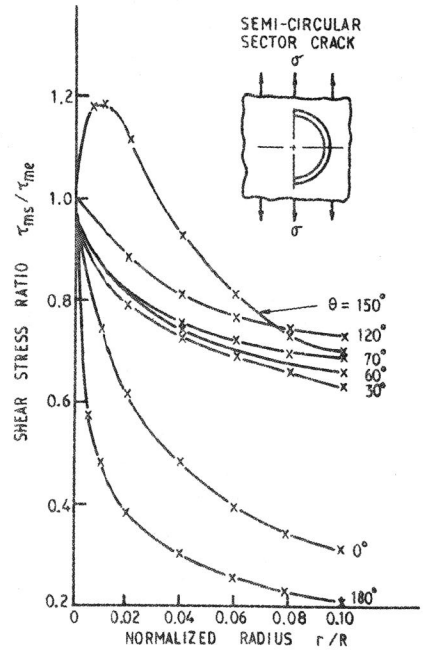


Figure 4 Variation of Shear Stress Ratio Versus Normalized Radius for $\alpha$ = 90 Deg.

In this paper, the terms "exact" and "singular" maximum shear stresses denoted respectively as $\tau_{me}$ and $\tau_{ms}$ are defined as the maximum shear stresses of Equation (4) computer respectively from Equations (1) and (2). Figs. 3 and 4 show the variation of the ratio ($\tau_{ms}/\tau_{me}$) of the singular ($\tau_{ms}$) to the exact ($\tau_{me}$) maximum shear stress versus the normalized radius (r/R) from the crack tip for the polar angle $\theta$ varying from zero to $\pi$ with an increment of 30 degrees. The maximum shear stresses of $\tau_{me}$ and $\tau_{ms}$ are computed using the exact solution of equation (1) and the singular-term solution of equation (2) respectively.

Based on the photoelastic method originally proposed by Irwin (3), a knowledge of the maximum shear stress at the angle $\theta_m$ corresponding to the radius $r_m$ is required to compute the stress intensity factor. These are provided in Figs. 5 and 6 showing the variation of the maximum shear stress ratio and the angle $\theta_m$ versus the normalized maximum radius $r_m/R$.

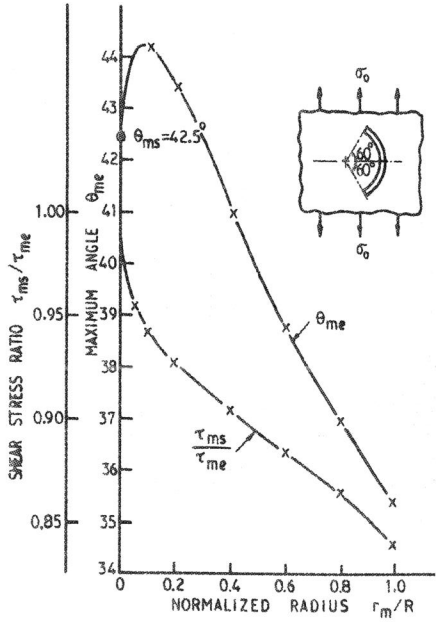


Figure 5 Variation of Maximum Angle $\theta_{me}$ and Corresponding Maximum Shear Stress Versus Normalized Radius for $\alpha$ = 60 Deg.

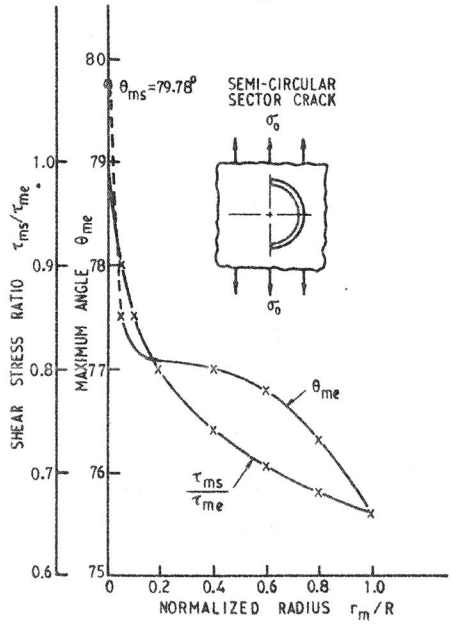


Figure 6 Variation of Maximum Angle $\theta_{me}$ and Corresponding Maximum Shear Stress Versus Normalized Radius for $\alpha$ = 90 Deg.



## EXPERIMENTAL DETERMINATION OF STRESS INTENSITY FACTORS

In order to illustrate the methods of analysis for the curved crack described in the above paragraph, two photoelastic experiments were performed to determine the mixed-mode stress intensity factors of $K_1$ and $K_2$. The geometry of the testpiece chosen is illustrated in Figure 7 with its

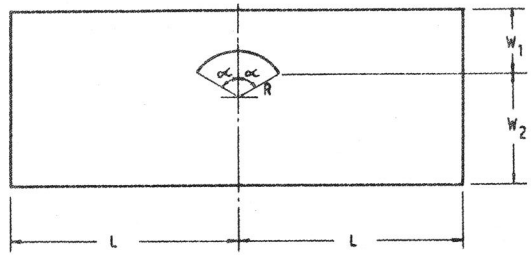


Figure 7 Specimen Geometry Used for Photoelasticity Analysis

dimensions outlined in Table I. The specimens were made of PSM-1 manufactured by Photoelastic Inc.

TABLE I Dimensions of Photoelastic Specimens

| No. | R | $\alpha$ | $W_1$ | $W_2$ | $W=W_1+W_2$ | L |
|---|---|---|---|---|---|---|
| 1 | 19.0 | 90° | 38.10 | 38.10 | 76.2 | 114.30 |
| 2 | 19.0 | 60° | 47.63 | 28.58 | 76.2 | 114.30 |

In the photoelastic determination of mixed-mode stress intensity factors of the circular-sector cracks, two methods (called I and II) are used to compare the computed values of $K_1$ and $K_2$ in the rectangular plate with those in an infinite plate.

For the Method I, photoelastic measurements are taken at two points near the crack tip or at the far-field region. The measured maximum shear stress $\tau_m$ is converted to the singular stress $\tau_m'$ by the following formula

$$\tau_m' = \tau_m \left(\frac{\tau_{ms}}{\tau_{me}}\right) \qquad (8)$$

where the maximum shear stress ratio of ($\tau_{ms}/\tau_{me}$) can be readily found from Figs. 3 and 4. The computed singular stress $\tau_m'$ is then substituted into Equation (6) for the solution of $K_1$ and $K_2$ values. Table II describes the computational procedures for the circular-sector cracks of half-angles 90 and 60 degrees.

TABLE II $K_1$ and $K_2$ Determination by Method I

| | 1 | 2 | 3 | 4 | 5 | 6 | 7 | 8 | 9 | 10 |
|---|---|---|---|---|---|---|---|---|---|---|
| No. | $\alpha$ | $r_1$ | $r_2$ | $\theta_1$ | $\theta_2$ | N | f KN/fr/mm | $\frac{\tau_m}{\sigma_o(2\pi)^{1/2}}$ | $\frac{(\tau'_m)_1}{\sigma_o(2\pi)^{1/2}}$ | $\frac{(\tau'_m)_2}{\sigma_o(2\pi)^{1/2}}$ |
| 1 | $90^o$ | 0.69 | 0.65 | $90^o$ | $60^o$ | 3 | 175 | 0.6822 | 0.5151 | 0.5082 |
| 2 | $60^o$ | 1.31 | 0.96 | $30^o$ | $60^o$ | 3 | 175 | 0.3898 | 0.343 | 0.3567 |

| | 11 | 12 | 13 | 14 | 15 | 16 |
|---|---|---|---|---|---|---|
| No. | $\frac{K_2}{K_1}$ | $\frac{K_{2\infty}}{K_{1\infty}}$ | $\frac{K_1}{\sigma_o(2\pi)^{1/2}}$ | $\frac{K_{2\infty}}{\sigma_o(2\pi)^{1/2}}$ | $\frac{K_{1\infty}}{\sigma_o(2\pi)^{1/2}}$ | $\frac{K_{2\infty}}{\sigma_o(2\pi)^{1/2}}$ |
| 1 | 0.0877 | 0.091 | 0.425 | 0.397 | 0.0372 | 0.036 |
| 2 | 0.628 | 0.638 | 0.245 | 0.2344 | 0.154 | 0.1496 |

Method II is based on the knowledge of the angle $\theta_m$ corresponding to the maximum radius $r_m$ within an isochromatic loop and the maximum shear stress $\tau_m$ of the loop to determine the stress intensity factors. As Equation (7) is derived from the singular stress equation, the conversion of the measured angle $\theta_m$ at the far-field region to the vicinity of the crack tip is achieved with

$$\theta'_m = \theta_m \left( \frac{\theta_{ms}}{\theta_{me}} \right) \qquad (9)$$

where the values of $\theta_{ms}$ and $\theta_{me}$ at different radii can be obtained from Figs. 5 and 6. The computed singular-term angle of $\theta'_m$ is then used to determine the ratio of $K_1/K_2$ from Equation (7). The maximum singular stress $\tau'_m$ can also be calculated using Equation (8) based on the measured value of $\tau_m$ corresponding to the angle $\theta_m$.

Finally, Equation (6) is used to determine the mixed-mode stress intensity factors of $K_1$ and $K_2$ from the computed values of $K_2/K_1$ and $\tau'_m$. The computational procedure for Method II is described in Table III.



TABLE III $K_1$ and $K_2$ Determination by Method II

| | 1 | 2 | 3 | 4 | 5 | 6 | 7 | 8 | 9 |
|---|---|---|---|---|---|---|---|---|---|
| No. | $\alpha$ | $r_m$ | $r_m/R$ | $\theta_m$ | N | f KN/fr/mm | $\theta'_m$ | $\frac{\tau_m}{\sigma_o(2\pi)^{1/2}}$ | $\frac{\tau'_m}{\sigma_o(2\pi)^{1/2}}$ |
| 1 | $90^o$ | 0.77 | 0.0404 | $78^o$ | 3 | 175 | $80.8^o$ | 0.6822 | 0.5144 |
| 2 | $60^o$ | 1.35 | 0.07067 | $37.8^o$ | 3 | 175 | $42.6^o$ | 0.3898 | 0.3411 |

| | 10 | 11 | 12 | 13 | 14 | 15 |
|---|---|---|---|---|---|---|
| No. | $\frac{K_2}{K_1}$ | $\frac{K_{1\infty}}{K_{1\infty}}$ | $\frac{K_1}{\sigma_o(2\pi)^{1/2}}$ | $\frac{K_{1\infty}}{\sigma_o(2\pi)^{1/2}}$ | $\frac{K_2}{\sigma_o(2\pi)^{1/2}}$ | $\frac{K_{2\infty}}{\sigma_o(2\pi)^{1/2}}$ |
| 1 | 0.0815 | 0.091 | 0.442 | 0.397 | 0.036 | 0.036 |
| 2 | 0.636 | 0.638 | 0.2358 | 0.2344 | 0.150 | 0.1496 |

## CONCLUSIONS

Two methods for the photoelastic determination of the mixed-mode stress intensity factors for circular-sector cracks in finite width and length plate are described. Although the singular-term equations for an inclined straight crack and a circular-sector crack under the mixed mode loading condition are identical, different exact solutions must be employed to convert the far-field photoelastic measurements to the singular solution. The results obtained from both methods illustrate that the application of photoelastic method can be successfully extended to the circular-sector cracks for determining the mixed-mode stress intensity factors by transferring the far-field stresses to the singular solution. The validity of the methods has been verified by performing two experiments and satisfactory agreement in the results is achieved with the proposed methods.

Notch effect on the photoelastic determination of mixed-mode stress intensity factors are well known (10-13). In certain crack configurations, the distortion of the angle $\theta_m$ and $\tau_{max}$ due to the notch effect can be significant (13). However, Method I is free from such notch distortion effects and is considered to be the preferred method over Method II.

## REFERENCES


[1] Sih, G.C., Handbook of Stress Intensity Factors, Institute of Fracture and Solid Mechanics, Leigh University, U.S.A. (1973).

[2] Tada, H., Paris, P.C. and Irwin, G.R., The Stress Analysis of Cracks Handbook, Del Research Corp., U.S.A. (1973).

[3] Irwin, G.R., The Dynamic Stress Distribution Surrounding a Running Crack - A Photoelastic Analysis, Proceedings Society Experimental Stress Analysis, 16, 93-96, (1958).

[4] Bradley, W.B. and Kobayashi, A.S., An Investigation of Propagating Cracks by Dynamic Photoelasticity, Experimental Mechanics, 10, 106-114. (1970).

[5] Smith, D.G. and Smith, C.W., Photoelastic Determination of $K_I$ Stress Intensity Factors, Engineering Fracture Mechanics, 4, 357-366 (1972).

[6] Theocaris, P.S. and Gdoutos, E.E. A Photoelastic Determination of $K_I$ Stress Intensity Factors, Engineering Fracture Mechanics, 7, 331-339, (1975).

[7] Gdoutos, E.E. and Theocaris, P.S., A Photoelastic Determination of Mixed-mode Stress-intensity Factors, Experimental Mechanics, 87-95 (1978).

[8] Etheridge, J.M. and Dally, J.W., A Three-parameter Method for Determining Stress Intensity Factors from Isochromatic Fringe Loops, Journal of Strain Analysis, 13, 91-94 (1978).

[9] Muskhelishvili, N.I., Some Basic Problems of the Mathematical Theory of Elasticity, P. Noordhoff Ltd., Holland, 1953.

[10] Schroedl, M.A., McGowan, J.J. and Smith, C.W., An Assessment of Factors Influencing Data Obtained by Photoelastic Stress Freezing Technique for Stress Fields Near Crack Tips, Engineering Fracture Mechanics, 4, 801-809 (1972).

[11] Schroedl, M.A., McGowan, J.J. and Smith, C.W., Determination of Stress Intensity Factors from Photoelastic Data with Applications to Surface-flaw Problems, Experimental Mechanics, 14, 392-399 (1974).

[12] Schroedl, M.A. and Smith, C.W., A Study of Near and Far Field Effects in Photoelastic Stress Intensity Determination, Engineering Fracture Mechanics, 7, 344-355 (1975).

[13] Chow, C.L. and Chan, W.Y., Notch Effects on Photoelastic Determination of Mixed-mode Stress Intensity Factors, Engineering Fracture Mechanics, 12, 253-265 (1979).